A small molecule that inhibits the evolution of antibiotic resistance

Anna Johnson*, Harrison Bracey*, Angel Joel Hernandez Viera, Juan Carvajal-Garcia, Esra Simsek, Kwangho Kim, Houra Merrikh[#]

Vanderbilt University School of Medicine, Department of Biochemistry, Nashville, TN, USA

*These authors contributed equally to this work.

[#]Corresponding author

Email: houra.merrikh@vanderbilt.edu

Summary

Antimicrobial resistance (AMR) rapidly develops against almost all available therapeutics. New antibiotics target essential processes in bacteria but fail to address the root of the problem: mutagenesis and subsequent evolution. We recently proposed that inhibiting evolution is the ultimate solution to preventing AMR development. Here, we describe the first compound that inhibits the evolution of AMR by directly targeting a highly conserved evolvability factor, Mfd. We previously found that this RNA polymerase-associated translocase is required for rapid AMR development across highly divergent pathogens. Through an *in vivo* screen of novel compounds, we identified a small molecule (referred to as ARM-1) that binds Mfd and prevents its RNA polymerase termination activity. Inhibition of Mfd activity by ARM-1 delays the development of mutations, both in pure culture and during infection. Importantly, our data show that ARM-1 prevents the evolution of AMR across highly divergent pathogens, including *Pseudomonas aeruginosa* and *Staphylococcus aureus*, which cause extremely difficult to treat infections due to AMR development. In summary, we describe a novel compound that could be developed into a clinically usable “anti-evolution” drug. This work shows that the mechanisms accelerating evolution are druggable, and that this strategy could prevent AMR development in the clinic.

Main Text

Antimicrobial resistance (AMR) is among the top five global health crises of the modern world. World Health Organization priority pathogens such as methicillin-resistant *Staphylococcus aureus* (MRSA) and drug-resistant *Mycobacterium tuberculosis* (DR-TB), along with hundreds of other drug resistant bacterial species, account for global mortality rates over 10 million every year[1]. By 2050, if unchecked, AMR is projected to cost 210 trillion USD in annual global GDP, with roughly 16.7 trillion from DR-TB alone.

We and others' previously proposed a fundamental shift in the approach to combatting AMR. Inhibiting evolution by directly inactivating the mechanisms that increase mutation rates could prevent the development of AMR during the treatment of infections. Our previous work showed that Mfd, an RNA polymerase (RNAP)-associated DNA translocase, increases mutagenesis and accelerates evolution of resistance across highly divergent species[2–4]. In this work, we describe our discovery of a novel small molecule that inactivates the evolvability factor, Mfd, demonstrating both that targeting bacterial evolvability factors directly is possible and can prevent the development of AMR during treatment of infections.

To determine if Mfd's activity and/or RNAP termination function could be inactivated through the use of a small molecule, we conducted a high-throughput *in vivo* screen of roughly 250,000 novel compounds. To identify such compounds, we modified a previously described system to reveal Mfd-specific inhibitors (Fig. 1a, Extended Data Fig. 1)[5]. The screen was designed such that we would only identify small molecules that are able to permeate bacterial cells and have little or no bactericidal activity or toxicity to mammalian cells. We used Δ*mfd Escherichia coli* cells containing a reporter system encoded on two different plasmids. One plasmid contains a *lac* operator (*lacO*) encoded directly upstream of the *lux* operon, which expresses proteins that produce luciferase, leading to readily detectable luminescence. The second plasmid expresses the *Salmonella enterica* serovar Typhimurium Mfd protein under the control of an IPTG-inducible promoter. The LacI protein, which binds to *lacO,* is a barrier to transcription; RNAP is unable to readily pass the bound protein and therefore the transcription machinery stalls. The stalled RNAP is quickly recognized by Mfd and is pushed off

the DNA. However, LacI "breathes" on and off DNA at a significant rate[6]. If Mfd is not present, or its activity is inhibited by a small molecule, the stalled RNAP will be able to proceed through the *lux* operon during the temporary dissociation of LacI from the operator sequence, leading to the production of luminescence (Fig 1a). Using this property, we measured relative luminescence in the presence of each compound to look for Mfd inhibition in this *in vivo* screen (Fig. 1a, Extended Data Fig. 1). To ensure that the observed changes were not due to potential off target effects, we assayed control strains carrying plasmids that did not contain the *mfd* gene and examined IPTG-dependence of the observed effects in parallel with the experimental conditions. Positive hits from this system are those which result in high luminescence only when transcription is induced and Mfd is present, and do not show prohibitive bactericidal or cytotoxic effects (Extended Data Fig. 1, 5). This approach led us to discover a novel compound that inhibited Mfd, which hereafter we refer to as ARM-1 (Anti-Resistance Molecule 1). The structure of ARM-1 (VU001) is shown in Fig. 1b.

As many commercially available compounds can have impurities, we synthesized ARM-1 to ≥99% purity (see Supplementary Information) and repeated the experiments performed in the screen prior to further investigation into the compound's effects on Mfd function. For our experiments, we synthesized this compound following an original synthesis strategy and thoroughly validated our product prior to proceeding (for synthesis description and compound validation, see Supplemental Information). We found that ARM-1 binds to Mfd with a k_d of 4.25μM (Fig. 2a), a notably tight binding affinity for a lead compound prior to medicinal chemistry optimization. This allowed us to use relatively low concentrations of ARM-1 in *in vivo* assays, effectively circumventing any potential bactericidal or cytotoxic effects. Using the same system employed for the high throughput screen, we measured and confirmed the effect of ARM-1 on Mfd's translocase activity. Treating cells with 50 to 100 μM ARM-1 resulted in a 3- to 5-fold inhibition of translocase activity *in vivo*. Given that there was no effect of ARM-1 on luminescence in cells lacking Mfd, we conclude that the effects of ARM-1 are directly through inhibition of Mfd (Fig. 1c).

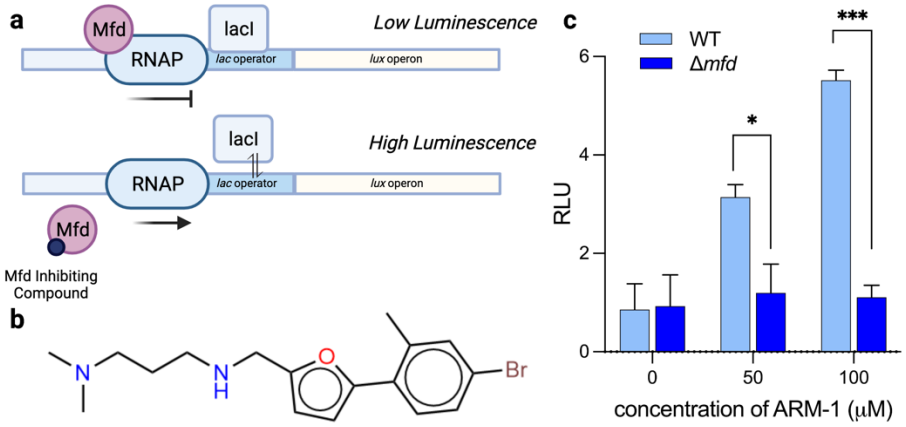

Figure 1: *In vivo* high throughput screen identifies lead compound ARM-1. a Schematic of *in vivo* screen design. In the upper panel, when Mfd is present, RNAP complexes stalled at the lacI-bound operator sequence are quickly removed, resulting in little to no transcription of the *lux* operon and low luminescence output. In the lower panel, when Mfd is either absent or inhibited, RNAP complexes stalled at the operator are not removed and are able to proceed during temporary dissociation of LacI, resulting in relatively high levels of luminescent output. **b** Structure of the lead compound, ARM-1. **c** Translocase activity assay showing relative luminescent output for WT and Δ*mfd S. typhimurium* ST19 strains containing the *in vivo* system with increasing concentrations of ARM-1. Relative luminescence is normalized to no compound and 0.5% DMSO solvent control. * $p < 0.05$ *** $p < 0.001$.

Mfd translocates along double-stranded DNA and dislodges stalled RNAP complexes[7,8]. As both processes have been demonstrated to be dependent on Mfd's ability to hydrolyze ATP, we directly examined the effect of ARM-1 on *in vitro* ATP hydrolysis by Mfd[9,10]. At dosages ranging from 6.25μM to 50μM ARM-1, at ratios of 125 to 1000 ARM-1 per Mfd, we observe a slight dose-dependent increase ATP hydrolysis (Fig. 2b, Supplemental Information Table S2). In the presence of ARM-1, ATP turnover by Mfd is not inhibited. In fact, the ATPase activity is enhanced almost 3-fold in the presence of 50μM ARM-1 (Fig. 2b, Extended Data Table 1). Together, these results suggest that Mfd acts on RNAP not only through enzymatic activity, but also through an allosteric mechanism, which is common to transcription terminators such as Rho[11,12,13].

To further investigate the mechanism by which ARM-1 inhibits Mfd activity, we performed a slightly modified version a of previously described *in vitro* RNA polymerase displacement assay[14]. In this assay, *E. coli* RNAP holoenzyme is stalled by CTP starvation on a short, radiolabeled DNA fragment containing a constitutively active promoter (see Methods). The first guanine encoded on this DNA fragment is 21 nucleotides downstream of the promoter. In the absence of CTP, RNAP stalls at this location. This stalled RNAP can then be removed by Mfd. As has been observed previously, when we performed this displacement assay with purified proteins, two DNA-protein complexes were observed by electrophoretic mobility shift assay (EMSA): a slower migrating initiation complex (IC), and a faster migrating elongation complex (EC)[14,15]. When quantified, we observed a ratio of EC to IC of consistent with prior work[10,16,17]. Addition of purified Mfd removed the stalled RNA polymerase, which results in a reduction of the ratio of ECs compared to ICs. We reason that when removed by Mfd, the displaced RNAP is free to re-bind the promoter, which is apparent by the increase in the amount of ICs (Fig. 2c, EC/IC=0.33). In contrast, when we pre-incubated Mfd with ARM-1, though we still observed a decrease in the amount of EC when compared to the reaction without Mfd, we no longer observed the corresponding increase in ICs (EC/IC=0.46), which is normally a downstream result of Mfd's RNAP removal function. This indicates that ARM-1 indeed inhibits Mfd's function by interfering with its ability to remove stalled RNAPs from DNA. The reduction in the ECs in the presence of ARM-1 is most likely due to the fact that at equilibrium, when RNAP cannot dissociate from DNA, it cannot re-initiate transcription, consequently preventing new EC formation. Importantly, the effects of ARM-1 in these experiments are not due to off target effects on RNAP. In our control reactions, ARM-1 did not have any detectable changes on RNAP complexes in the absence of Mfd (Fig 2c).

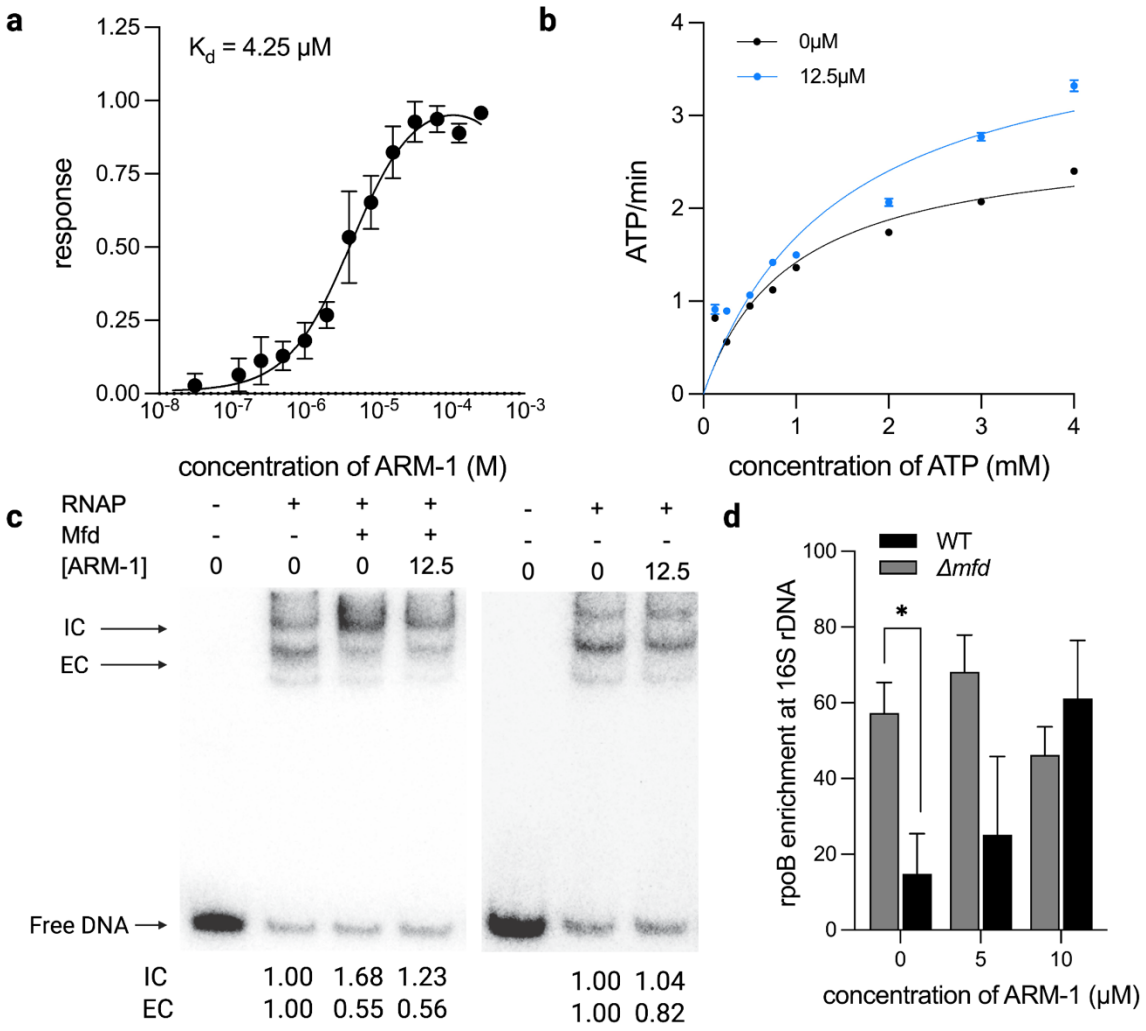

Figure 2. ARM-1 affects Mfd's RNAP modulation activity. a k_d of ARM-1 was determined using microscale thermophoresis. Data show represent a minimum of three independent experiments. **b** NADH-coupled ATPase assay[18]. ATP hydrolysis by Mfd was coupled to NADH oxidation. Phosphoenolpyruvate is converted to pyruvate by pyruvate kinase, transferring a phosphate group onto ADP, which is only present in the reaction following ATP hydrolysis by Mfd. Pyruvate is then converted to lactate by lactate dehydrogenase, oxidizing NADH to NAD^+. Absorbance at 340nm by NADH is used to monitor the reaction. Data shown represent a minimum of 3 biological replicates. **c** Transcription roadblock assay. A P32-labled 176bp PCR fragment was incubated with *E. coli* RNAP along with saturating concentrations of ATP, GTP, and UTP. 100nM *S. typhimurium* ST19 Mfd preincubated with indicated concentrations of ARM-1 was added and the reaction allowed to proceed for 6 minutes. DNA products were then resolved on a polyacrylamide gel and analyzed by

phosphorimaging. On the left gel, Lane 1 shows no enzyme and no compound control. Lanes 2 and 3 show RNAP alone and RNAP with Mfd, respectively, both in the absence of ARM-1 treatment. Lanes 4 shows RNAP and Mfd in the presence 12.5μM ARM-1. On the right gel, Lane 1 shows the no enzyme and the no compound control, Lane 2 shows RNAP alone, and Lane 3 shows RNAP with 12.5μM ARM-1. Quantification of these gels is shown below each lane. Analysis was performed using Image Lab 6.0.1. Data shown representative of at least two separate experiments. **d** ChIP-qPCR of RpoB at 16S rDNA. *S. typhimurium* ST19 of indicated genotype grown to mid exponential phase in cells treated with indicated concentration of ARM-1 for 2 generations prior to harvest. ChIP was performed using 8RB13 monoclonal antibody against RpoB. Data shown are representative of 3 biological replicates. * $p < 0.05$

We next investigated the effect of ARM-1 on Mfd *in vivo*. For this, we performed chromatin immunoprecipitations (ChIPs) of the β subunit of RNAP (RpoB) in WT and Δ*mfd S. typhimurium* ST19 strains, treated with ARM-1 for at least two generations of exponential growth. In the untreated condition, we observe an increase in RpoB association with rDNA, a highly transcribed region of the bacterial genome, in the absence of Mfd (Fig. 2e, Extended Data Fig. 3). This effect is consistent with Mfd's function in displacing stalled elongation complexes, particularly at regions that are difficult to transcribe[19]. At 5mM ARM-1, there is little change in RpoB association, but at 10mM there is a dramatic decrease in association of RpoB in WT cells, consistent with Mfd inhibition and extended occupancy of elongation complexes at the target region (Fig. 2e, Extended Data Fig. 3). In the Δ*mfd* background, contrary to our expectations, RpoB enrichment in not significantly different from WT in the absence of ARM-1. This suggests, consistent with our observations from the transcription roadblock assay *in vitro*, that ARM-1 may have a limited effect on elongating RNAP complexes independent of Mfd (Fig. 2d *right panel*, 2e). Because we observe no growth defects at these concentrations of ARM-1, these patterns are unlikely to be due to indirect effects such as changes in transcription levels (Extended Data Fig. 6). In summary, these data support a nuanced effect of ARM-1 on Mfd's biochemical activity both *in vitro* and *in vivo*.

Our lab has previously shown that the mutagenic effect of Mfd is conserved during bacterial infection of eukaryotic cells. Luria-Delbruck assays have demonstrated that mutation rates are increased by Mfd across highly divergent bacterial species[2]. With ARM-1 treatment, we observe a 3-fold reduction in WT *S. typhimurium* ST19 mutation frequency, consistent with direct inhibition of Mfd (Fig. 3a). To determine if ARM-1 can also reduce mutagenesis during infection, we infected HeLa cells with wild-type and Δ*mfd S. typhimurium* ST19, and measured mutation frequency through acquisition of 5-fluorocytosine resistance[2,20]. The compound was added to the culture media following invasion to ensure uniform treatment conditions. We observed an almost 7-fold decrease in mutation frequency in the absence of Mfd (Fig. 3c). WT *S. typhimurium* cells have a mutation frequency of 22.3 mutations per 10^5 bacteria during infection, whereas Δ*mfd* strains have a 3.3 mutations per 10^5 bacteria during infection (Fig. 3c). We found that treatment with ARM-1 reduces WT mutation frequency to 3.2 mutations per 10^5 bacteria, a 7-fold reduction compared to untreated cells, which were consistent with rates we observe for Δ*mfd* strains (Fig. 3c). Neither the Δ*mfd* mutant nor ARM-1 or solvent-treated WT or Δ*mfd* strains show a defect in invasion or proliferation of HeLa cells (Fig. 3b). These observations confirm that the differences in mutation frequencies during infection are not due to altered growth dynamics. Furthermore, no cytotoxic effects of ARM-1 on HeLa cells were observed during the timeframe of this experiment, allowing for direct comparisons between ARM-1 untreated and treated infections (Extended Data Fig. 5). Taken together, these data strongly suggest that ARM-1 is directly inhibiting bacterial mutagenesis mechanisms during infection.

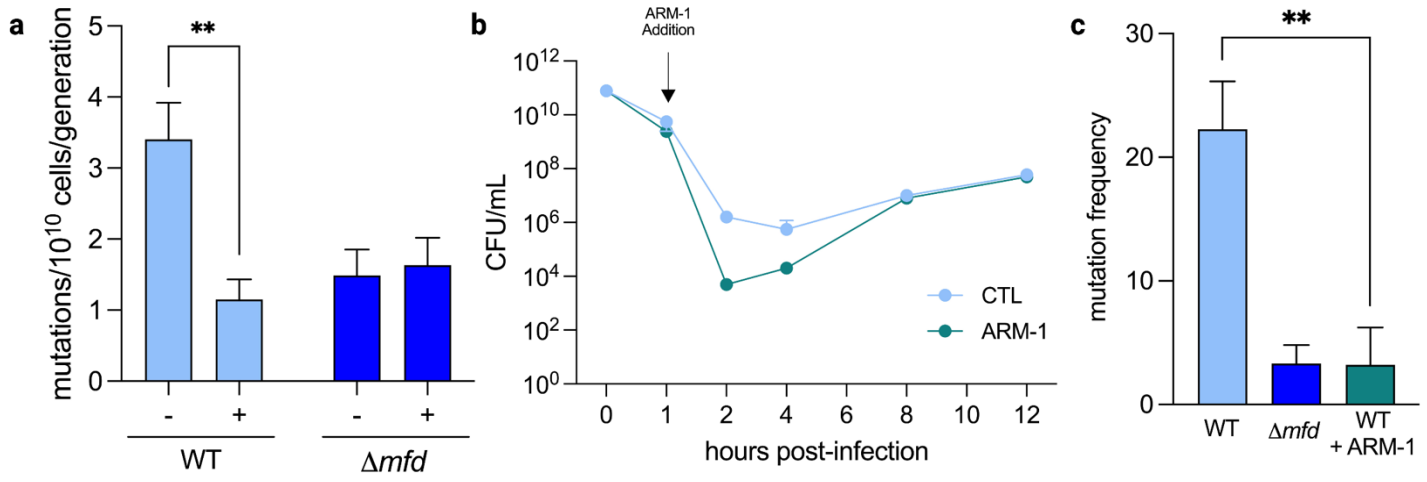

Figure 3. ARM-1 reduces mutation frequency in culture and during infection. a Luria-Delbruck fluctuation assay with ARM-1 treatment. Single colonies of WT and Δ*mfd S. typhimurium* ST19 were used to inoculate overnight cultures with appropriate antibiotic selection. Cultures were then diluted back to OD_{600} 0.0005 and grown to OD_{600} 0.5 with or without 100µM ARM-1 treatment. Samples were plated on 80ng/ml ciprofloxacin and grown overnight, then enumerated the following day. Data shown are the result of a minimum of 50 replicates. **b** Invasion and infection efficiency in the presence of ARM-1. WT *S. typhimurium* ST19 in mid-log phase growth was used to infect HeLa cells. Invasion was allowed to proceed for 1 hour before uninternalized bacteria were removed and fresh media applied, containing vehicle control or 31.25µM ARM-1. At the indicated timepoints, HeLa cells were lysed using 1% Triton-H_2O and intracellular bacteria serially diluted and plated on LB for CFU enumeration. **c** Mutation frequency post mammalian cell infection. WT and Δ*mfd S. typhimurium* ST19 were used to infect HeLa cells as described in **b** Following infection, intracellular bacteria were harvested and plated on 50µg/mL 5-fluorocytosine and grown overnight. Mutants were enumerated the following morning. Mutation frequency is shown as mutants per 10^5 bacteria harvested from HeLa lysates. Data shown are the result of a minimum of 3 biological replicates. ** $p < 0.01$

We next examined the effect of ARM-1 on the evolution of antibiotic resistance. Genetic deletion of the *mfd* gene reduces the rates and extent of resistance development in laboratory evolution experiments[2,21]. We assessed the impact of ARM-1 on resistance development across diverse pathogens and in response to multiple

classes of antibiotics. In these experiments, bacteria were challenged with increasing concentrations of antibiotic over a minimum of 55 generations. We observed a significant reduction in resistance development when bacteria were treated with ARM-1 compared to those that were untreated, in all species and antibiotics tested. In *S. typhimurium*, challenged with rifampicin or trimethoprim, we observed at minimum a 100-fold reduction in median minimum inhibitory concentration (MIC) between untreated and treated conditions in these experiments (Fig. 4a-b). This pattern was also observed in *P. aeruginosa*, *S. aureus*, and *L. monocytogenes*, with ARM-1 treatment resulting in 80, 800, and 1000 fold reduction in resistance to rifampicin, respectively (Fig. 4a). We observed very similar results when these bacteria were treated with trimethoprim (Fig. 4b). Sequencing of relevant resistance loci over the course of treatment confirmed that these observations are due to a reduction in mutations. Populations of cells that were treated with ARM-1 had significantly less mutations compared to untreated cells (Extended Data Table 1). Doubling time was consistent between treated and untreated populations across all species tested (Extended Data Fig. 6), indicating that our results are not simply attributable to growth defects.

To determine whether ARM-1 could be used to reduce evolution of AMR in cells that contain existing mutations that make them resistant to various antibiotics, we analyzed patient isolates of *S. typhimurium*, *S. aureus*, and *P. aeruginosa* which already carry resistance mutations to other antibiotics. We found that ARM-1 treatment still leads to a significant reduction in resistance development, suggesting that prior mutations that lead to AMR do not impact the effectiveness of ARM-1.

Ideally, cells should not be able to develop resistance to an anti-evolution drug. A compound that inhibits the mechanism underlying evolution should prevent resistance development to itself as well. To test this hypothesis, we treated cells with toxic levels of ARM-1 (without antibiotics), virtually killing all cells (Extended Data Fig. 6a), and measured changes in minimum inhibitory concentration (MIC) over time. We did not observe any changes in MIC or growth dynamics when *E. coli* or *S. aureus* were challenged with ARM-1 alone; the MIC remained constant at 400μM of ARM-1 even after 196 hours of exposure, which corresponds to 60 to 70

generations (Fig. 4c, Extended Data Fig. 6). This strongly suggests that bacteria are unlikely to evolve resistance to ARM-1 itself, which shows that this molecule is an "ideal" anti-evolution compound that should be developed into a drug for use in the clinic.

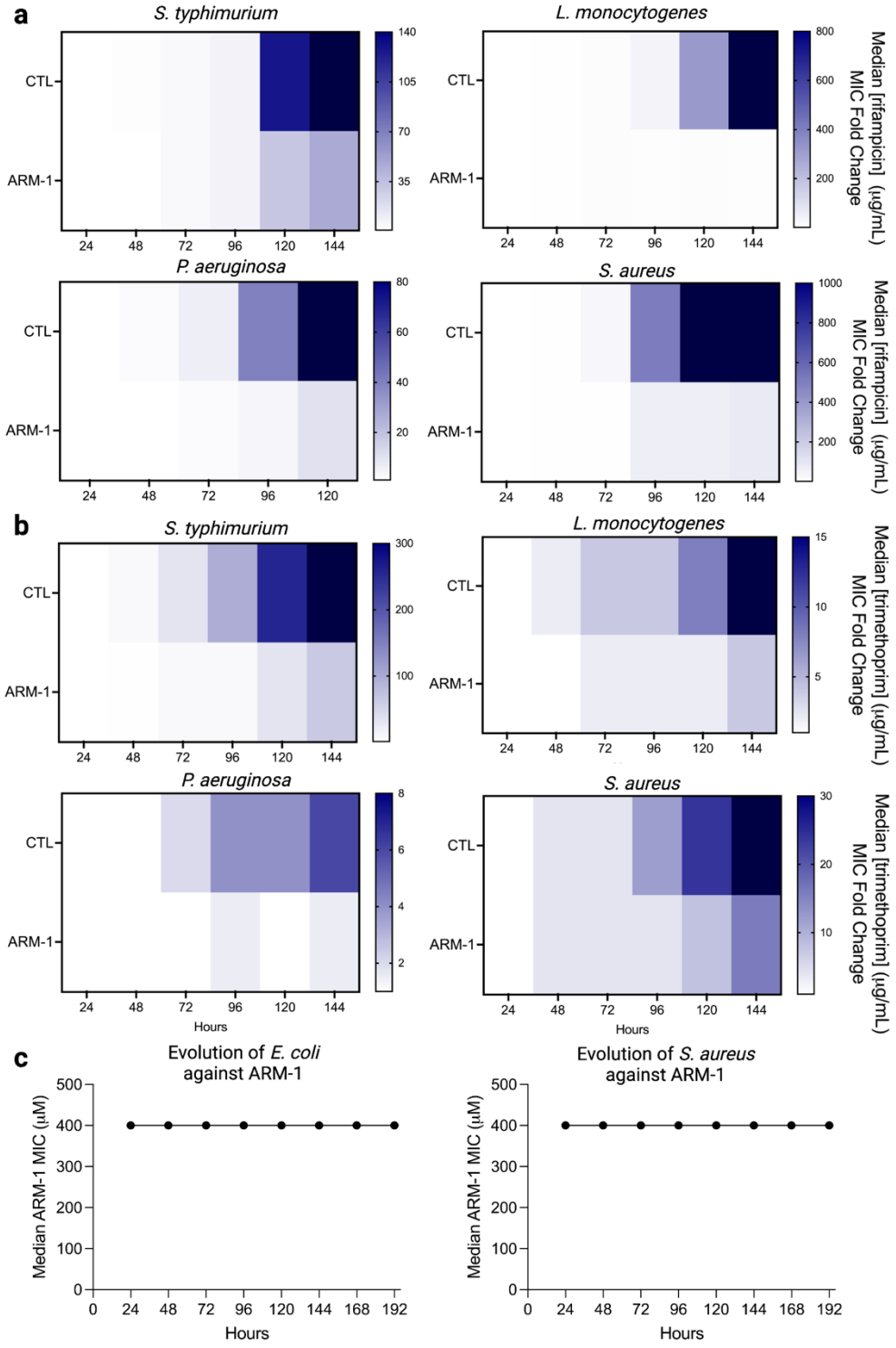

Figure 4. ARM-1 inhibits the evolution of antibiotic resistance. a-b Evolution of indicated species against **a** rifampicin and **b** trimethoprim in the presence of ARM-1. Heatmaps show median MIC over time. Concentrations are indicated to the right of each plot. Each strain and antibiotic is the result of at least 12 biological replicates. Concentration of ARM-1 used against *L. monocytogenes*, *P. aeruginosa*, and *S. aureus* is 100μM. Concentration of ARM-1 used against *S. typhimurium* is 50μM. Populations of bacteria are grown overnight in a series of increasing antibiotic concentrations, with or without ARM-1 present. The following day, the population from the highest tolerated concentration is re-challenged with higher concentrations of antibiotic. The median MIC is determined after each 24 hour growth (which corresponds to 7 to 10 generations) period as the lowest concentration of antibiotic at which at least 50% growth impairment is observed compared to an untreated population. MIC fold change is reported as the change in MIC from the first day of growth to each subsequent day. **c** Minimum inhibitory concentration of ARM-1 in *E. coli* and *S. aureus* after a minimum of 60 generations.

In addition to our discovery of ARM-1 and its impact on AMR, it is important to note that this work has provided a novel insight into Mfd function. Our *in vitro* and *in vivo* findings show that Mfd not only requires its ATPase hydrolysis activity to remove stalled RNAPs from DNA, but that it also harbors an allosteric mechanism that is essential for this process. In other words, it appears that Mfd's allosteric modulation of RNAP is essential for its function. This is consistent with previously characterized transcription terminators, which also use allosteric mechanisms to remove RNAP from DNA[13]. This finding makes a valuable contribution to the field and provides a new tool (ARM-1) to further study the mechanism by which Mfd removes RNAP from DNA.

The universal impact of ARM-1 on highly divergent bacteria strongly suggests that we may be able to develop a single drug that can be used against AMR development in many different pathogens. A single effective anti-evolution drug simplifies the development process. The development of ARM-1 for clinical use could provide us with one anti-evolution drug that can be used under many circumstances when AMR is a problem, regardless

of the treatment or the pathogen - including those that already carry resistance mutations such as multi-drug resistant strains of *Staphylococcus aureus* or *Mycobacterium tuberculosis*.

The findings described here - the discovery of ARM-1 - show that it is possible to inhibit the rise of AMR with a small molecule that could ultimately be developed into an anti-evolution drug. There are no therapies that are immune to mutagenesis, the driver of adaptative evolution. The discovery of new antibiotics and other therapies that kill cells is invaluable. However, when essential processes are inhibited either through antibiotics or other therapies that kill cells, we are in essence performing a genetic screen that selects for mutants which are resistant to that selection pressure. This inevitably places all novel treatments under the threat of adaptive evolution by pathogens. The ultimate solution to protecting the efficacy of new therapeutics and limiting the development of resistant infections is to inhibit the ability of bacteria to evolve resistance during treatment. Our discovery of ARM-1 sets the foundation for the development of anti-evolution drugs to combat the rise of AMR.

REFERENCES

1. Dadgostar P. Antimicrobial Resistance: Implications and Costs. *Infect Drug Resist*. 2019;12:3903-3910. doi:10.2147/IDR.S234610

2. Ragheb MN, Thomason MK, Hsu C, et al. Inhibiting the Evolution of Antibiotic Resistance. *Mol Cell*. 2019;73(1):157-165.e5. doi:10.1016/j.molcel.2018.10.015

3. Westblade LF, Campbell EA, Pukhrambam C, et al. Structural basis for the bacterial transcription-repair coupling factor/RNA polymerase interaction. *Nucleic Acids Res*. 2010;38(22):8357-8369. doi:10.1093/nar/gkq692

4. Park JS, Marr MT, Roberts JW. E. coli Transcription repair coupling factor (Mfd protein) rescues arrested complexes by promoting forward translocation. *Cell*. 2002;109(6):757-767. doi:10.1016/s0092-8674(02)00769-9

5. Chambers AL, Smith AJ, Savery NJ. A DNA translocation motif in the bacterial transcription–repair coupling factor, Mfd. *Nucleic Acids Res*. 2003;31(22):6409-6418. doi:10.1093/nar/gkg868

6. Du M, Kodner S, Bai L. Enhancement of LacI binding in vivo. *Nucleic Acids Res*. 2019;47(18):9609-9618. doi:10.1093/nar/gkz698

7. Brugger C, Zhang C, Suhanovsky MM, et al. Molecular determinants for dsDNA translocation by the transcription-repair coupling and evolvability factor Mfd. *Nat Commun*. 2020;11(1):3740. doi:10.1038/s41467-020-17457-1

8. Selby CP, Sancar A. Molecular mechanism of transcription-repair coupling. *Science*. 1993;260(5104):53-58. doi:10.1126/science.8465200

9. Kang JY, Llewellyn E, Chen J, et al. Structural basis for transcription complex disruption by the Mfd translocase. *Elife*. 2021;10:e62117. doi:10.7554/eLife.62117

10. Smith AJ, Pernstich C, Savery NJ. Multipartite control of the DNA translocase, Mfd. *Nucleic Acids Res*. 2012;40(20):10408-10416. doi:10.1093/nar/gks775

11. Song E, Uhm H, Munasingha PR, et al. Rho-dependent transcription termination proceeds via three routes. *Nat Commun*. 2022;13(1):1663. doi:10.1038/s41467-022-29321-5

12. Hao Z, Svetlov V, Nudler E. Rho-dependent transcription termination: a revisionist view. *Transcription*. 2021;12(4):171-181. doi:10.1080/21541264.2021.1991773

13. Roberts JW. Mechanisms of Bacterial Transcription Termination. *J Mol Biol*. 2019;431(20):4030-4039. doi:10.1016/j.jmb.2019.04.003

14. Carter RH, Demidenko AA, Hattingh-Willis S, Rothman-Denes LB. Phage N4 RNA polymerase II recruitment to DNA by a single-stranded DNA-binding protein. *Genes Dev*. 2003;17(18):2334-2345. doi:10.1101/gad.1121403

15. Smith AJ, Savery NJ. RNA polymerase mutants defective in the initiation of transcription-coupled DNA repair. *Nucleic Acids Research*. 2005;33(2):755-764. doi:10.1093/nar/gki225

16. Deaconescu AM, Chambers AL, Smith AJ, et al. Structural Basis for Bacterial Transcription-Coupled DNA Repair. *Cell*. 2006;124(3):507-520. doi:10.1016/j.cell.2005.11.045

17. Smith AJ, Szczelkun MD, Savery NJ. Controlling the motor activity of a transcription-repair coupling factor: autoinhibition and the role of RNA polymerase. *Nucleic Acids Res*. 2007;35(6):1802-1811. doi:10.1093/nar/gkm019

18. Kiianitsa K, Solinger JA, Heyer WD. NADH-coupled microplate photometric assay for kinetic studies of ATP-hydrolyzing enzymes with low and high specific activities. *Anal Biochem*. 2003;321(2):266-271. doi:10.1016/s0003-2697(03)00461-5

19. Ragheb MN, Merrikh C, Browning K, Merrikh H. Mfd regulates RNA polymerase association with hard-to-transcribe regions in vivo, especially those with structured RNAs. *Proc Natl Acad Sci U S A*. 2021;118(1). doi:10.1073/pnas.2008498118

20. Richardson AR, Soliven KC, Castor ME, Barnes PD, Libby SJ, Fang FC. The Base Excision Repair system of Salmonella enterica serovar typhimurium counteracts DNA damage by host nitric oxide. *PLoS Pathog*. 2009;5(5):e1000451. doi:10.1371/journal.ppat.1000451

21. Barlow M, Hall BG. Experimental prediction of the natural evolution of antibiotic resistance. *Genetics*. 2003;163(4):1237-1241.

Methods

Bacterial Strains

Organism	Source	Identifier
S. typhimurium ST19	Hayden et al., 2016	HM1996
S. typhimurium ST19, *mfd*	Ragheb et al, 2019	HM3429
S. aureus, patient isolate	Vanderbilt University Medical Center	HM4318
L. monocytogenes	This study	HM3274
L. monocytogenes, *mfd*	This study	HM3702
E. coli K12	This study	HM1347
P. aeruginosa	Wolfgang et al., 2003	HM2212
E. coli NM525 Δ*mfd* +pRCB-Nluc + pUC19	This study	HM3418
E. coli NM525 Δ*mfd* +pRCB-Nluc +pUC19-ST19mfd	This study	HM3419
E. coli NM525 Δ*mfd* +pRCB-Nluc +pUC19-ST19-L499Rmfd (RID)	This study	HM3420
E. coli pCA24N IPTG inducible Mfd-6xHis	Gift from Dr. Evgeny Nudler	HM3787

Mammalian Cell Lines

Strain	Source	Identifier
HeLa	ATCC	CCL-2
Caco-2	ATCC	HTB-37
HEK293	ATCC	CRL-1573

Plasmids

Name	Source	Identifier
pRCB-Nluc	Gift from Drs. Nigel Savery and Seth Darst	N/A
pUC19	Addgene	#50005

Preparation of ARM-1 (VU0934184); see Extended Data Figs. 7-9

Materials: Solvents were obtained from either an MBraun MB-SPS solvent system or freshly distilled (tetrahydrofuran was distilled from sodium-benzophenone; toluene was distilled from calcium hydride and used immediately; dimethyl sulfoxide was distilled from calcium hydride and stored over 4 Å molecular sieves). Commercial reagents were used as received. The molarity of *n*-butyllithium solutions was determined by titration using diphenylacetic acid as an indicator (average of three determinations).

Instrumentation: Semi-preparative reverse phase HPLC was conducted on a Waters HPLC system using a Phenomenex Luna 5 μm C18(2) 100A Axia 250 x 10.00 mm column or preparative reverse phase HPLC (Gilson) using a Phenomenex Luna column (100 Å, 50 x 21.20 mm, 5 μm C18) with UV/Vis detection. Infrared spectra were obtained as thin films on NaCl plates using a Thermo Electron IR100 series instrument and are reported in terms of frequency of absorption (cm^{-1}). ^{1}H NMR spectra were recorded on Bruker 400, 500, or 600 MHz spectrometers and are reported relative to deuterated solvent signals. Data for ^{1}H NMR spectra are reported as follows: chemical shift (δ ppm), multiplicity (s = singlet, d = doublet, t = triplet, q = quartet, p = pentet, m = multiplet, br = broad, app = apparent), coupling constants (Hz), and integration. ^{13}C NMR spectra were recorded on Bruker 100, 125, or 150 MHz spectrometers and are reported relative to deuterated solvent signals. LC/MS was conducted and recorded on an Agilent Technologies 6130 Quadrupole instrument.

Compound preparation:

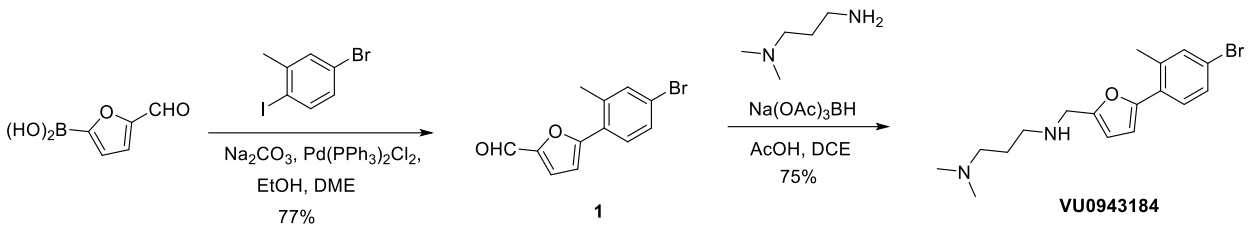

Compound 1. (5-formylfuran-2-yl)boronic acid (1.0 g, 7.15 mmol), 4-bromo-1-iodo-2-methylbenzene (1.63 g, 5.50 mmol), sodium carbonate (2 mL, 2 M solution), and bis(triphenylphosphine)palladium(II) dichloride (193 mg, 0.28 mmol) were added to pressure vessel and dissolved in dimethoxyethane (2 mL) and ethanol (3.5 mL). The solution was sparged with argon for 5 minutes, and the reaction was then sealed and heated to 65 °C for 12 hr. The reaction was then cooled to room temperature and diluted into ethyl acetate/H_2O (30 mL, 1:1). The organic layer was separated, and the aqueous layer was extracted with ethyl acetate (3 x 30 mL). The combined organic layers were dried over $MgSO_4$, filtered, and concentrated *in vacuo*. The crude product was purified by ISCO column chromatography eluting with 0 to 40% EtOAc in hexanes to afford the brown solid title compound **1** (1.13 g, 77 % yield). ^{1}H NMR (400 MHz, CDCl3) δ 9.68 (s, 1 H), 7.67 (d, *J* = 8.4 Hz 1 H), 7.46-7.41 (m, 2H), 7.33 (d, *J* = 3.6 Hz 1 H), 6.74 (d, *J* = 3.6 Hz 1 H), 2.53 (s, 3 H).

VU001. To a solution of compound 1 (0.5 g, 1.89 mmol) in dichloromethane (8 mL) was added N,N-dimethylpropane-1,3-diamine (0.25 g, 2.45 mmol). After stirring 2 h at room temperature, sodium triacetoxyborohydride (0.44 g, 2.08 mmol) and acetic acid (0.8 mL) were added to reaction mixture. The reaction mixture was stirred for 16 hr at room temperature, quenched with sat. sodium bicarbonate (20 mL), extracted with dichloromethane (3 x 30 mL). The combined organic phase was dried over $MgSO_4$, filtered, and concentrated *in vacuo*. The crude product was purified by ISCO column chromatography eluting with 0 to 70% MeOH in dichloromethane to afford the yellow oil product (0.29 g, 44% yield). ^{1}H NMR (400 MHz, CD_3OD) δ 7.63 (d, *J* = 8.4 Hz, 1H), 7.44 (s, 1H), 7.39 (dd, d, *J* = 8.4, 1.6 Hz, 1H), 6.60 (d, *J* = 3.6 Hz, 1H), 6.42 (d, *J* = 3.6

Hz, 1H), 3.83 (s, 2H), 2.67 (t, *J* = 7.2 Hz, 2H), 2.48 (s, 3H), 2.37 (t, *J* = 7.2 Hz, 2H), 2.25 (S, 6H), 1.73 (p, *J* = 7.6 Hz, 2H); LCMS calc'd for C17H23BrN2O $[M+H]^+$: 351.3 measured 352.4.

High-Throughput Screen (Calibr)

Workflow for the primary screen is described in the main text, with additional details provided in Extended Data Fig. 1. This screen was performed by Calibr (Scripps Research Institute).

S. typhimurium Mfd Purification

S. typhimurium Mfd was purified by growing up HM3787 cells overnight from a single colony in LB + 20 µg/mL chloramphenicol with agitation at 37°C. The next day 1 L of fresh LB + chloramphenicol was inoculated with 10 mL of overnight culture, incubated with agitation at 37°C. at optical density of 0.3 1 mM of IPTG was added and growth was continued for another 4 hours. Cells were then centrifuged at 5,000 rpm for 10 min and washed with PBS. Cell paste was then resuspended in 30 mL HisTrap lysis buffer (50 mM $NaPO_4$ pH = 8.0; 0.5 mM DTT; 0.5 M NaCl; 5 mM imidazole pH = 8.0) plus 2x Roche inhibitor proteases pills and homogenized. Cells were sonicated at midi-tip for 5 minutes at 50% amplitude with 30 second pulse intervals in an ice bath then centrifuged at 15,000 rpm for 30 minutes at 4°C. Supernatant was loaded on a His-Trap column (6 mL) in the same buffer, washed with NiWash Buffer (50 mM $NaPO_4$, 300 mM NaCl, and 40 mM imidazole pH 7.4), then eluted with NiElution Buffer (50 mM $NaPO_4$, 300 mM NaCl, and 150 mM imidazole pH7.4). One 15 mL fraction was collected and dialyzed overnight in a Slide-A-Lizer (Thermo Scientific) against 1000 mL of TGED Buffer (10 mM Tris-HCl pH = 8.0; 5% glycerol; 0.1 mM DTT; 0.1 mM EDTA; 50 mM NaCl). Dialysis material was centrifuged at 15,000 rpm for 30 minutes at 4°C. Using an AKTA system supernatant was loaded at 3x Heparin (1 mL) columns (GE) in TGED Buffer + 50 mM NaCl buffer at 0.6 mL/min (pressure 0.5 mPa) and eluted by the same buffer with 1 M NaCl in linear gradient from 0% to 100% in 20 column volumes. Fractions were 1 mL during loading and 1 mL during separation. Peaks with a correct molecular weight from Heparin purification were diluted to 50 mL in TGED buffer without NaCl and loaded at MonoQ 5/50 column (GE) in TGED buffer + 50 mM NaCl buffer at 2 mL/min (pressure 3.4 mPa) and eluted by the same buffer with

1 M NaCl in linear gradient from 0% to 100% in 20 column volumes. Fractions were 1 mL during loading and 0.5 mL during separation. Eluate was dialyzed overnight against 1000 mL of 10 mM RA Buffer (10 mM HEPES, 1 mM DTT, 50% glycerol, 1 mM EDTA, 500 mM KCl, and 40 mM $MgCl_2$ pH 8.0) in a Slide-A-Lyser. Resulting solution was aliquoted in 0.1 mL parts and flash-frozen in liquid nitrogen before being stored at -80°C.

Translocase Assay

HM3418 (*E. coli* NM525 Δ*mfd* +pRCB-Nluc + pUC19) and HM3419 (*E. coli* NM525 Δ*mfd* +pRCB-Nluc +pUC19-ST19mfd) were grown overnight from single colonies in the presence of antibiotic selection. Overnight cultures were back-diluted the following morning to OD600 0.05, then grown in the presence or absence of ARM-1 at 37°C until cultures reach OD600 0.50. In a 96-well plate, 80µL of cells from each sample were combined with 100µL LB and 20µL of luminescence reporter substrate (NanoLuc, Promega). Luminescence of each well quantified on a BioTek SynergyNeo plate reader.

Binding Affinity Analysis

Microscale thermophoresis was performed on a Monolith (NanoTemper). Purified Mfd was His-tagged labeled using NanoTemper's His-Tag Labeling Kit (MO-L018) according to manufacturer's protocol. Serial 1:2 dilutions were made of C5 starting with an end concentration of 1 mM in PBST buffer for a total of 16 dilutions. Labeled Mfd was then added to each dilution with an end concentration of 50 nM. MST experiments were performed under default settings apart from fluorescence intensity set to 100%. The raw data was imported into Prism 9 software and nonlinear regression was used to find the K_d.

NADH-Coupled ATPase Assay

ATPase assays were performed as described in Kiiansita et al., 2003. All reactions were performed at 37°C in a 150µL reaction volume in a 96 well plate. Reactions were performed in repair buffer (40 mM HEPES pH 8.0, 100 mM KCl, 8 mM $MgCl_2$, 4% glycerol (v/v), 5 mM DTT and 100 µg/ml BSA) supplemented with 4.4 units

pyruvate kinase, 5.7 units lactate dehydrogenase, 500 μM phosphoenolpyruvate and 400 μM NADH. Mfd in a final concentration of 50nM and ARM-1 (aqueous solution, pH 8.0) in varying concentrations were added at least 15 minutes prior to starting reaction and allowed to incubate on ice. To start reaction, varying quantities of ATP were added and absorbance at 340nm was measured every 60 seconds for 1 hour in an Epoch2 microplate spectrophotometer (BioTek).

RNAP Displacement Assay

5 ng of a ^{32}P labeled, 176 bp PCR fragment containing the promoter of the ampicillin resistance gene from pDR110, a gift from David Rudner, were incubated with 1 unit of E. coli RNA Polymerase holoenzyme (NEB) for 15 mins at 37 °C. Then, NTPs were added to a final concentration of 1.7 mM (ATP) or 80 uM (UTP, GTP), as well as 80 uM ApU (Jena Bioscience), and incubated for 15 mins at 37 °C. Purified *S. typhimurium* ST19 Mfd (final concentration of 100 nM) that had been pre-incubated for 10 mins at 37 °C with the indicated amounts of ARM-1 (aqueous solution, pH 8.0) was added and incubated for 6 mins at 37 °C. 4 ul of the reaction were loaded into a polyacrylamide gel that had been pre-run for 45 mins at 70 V, and run for 55 mins at 150 V on ice, using 1X TBE buffer. The products were analyzed by phosphorimaging (GE Healthcare) and quantified using Image Lab 6.0.1.

Template Sequence:

TTAGACGTCAGGTGGCACTTTTCGGGGAAATGTGCGCGGAACCCCTATTTGTTTATTTTTCTAAAT
ACATTCAAATATGTATCCGCTCATGAGACAATAACCCTGATAAATGCTTCAATAATATTGAAAAAG
GAAGAGTATGAGTATTCAACATTTCCGTGTCGCCCTTATTCCCT

Evolution Assays

Evolution experiments were performed for the indicated strains. For *S. typhimurium*, *S. aureus*, *L. monocytogenes*, *P. aeruginosa*, and *E. coli*, overnight cultures, started from a single colony, were back diluted to OD600 = 0.005 and used to inoculate a 96-well plate. Cells were grown for 24 hours with agitation, at 37°C,

in LB with a gradient of concentrations of the indicated antibiotic to select for resistance. Optical densities were subsequently measured in an Epoch2 microplate spectrophotometer (BioTek). Cultures that grew (defined by at least 50% growth relative to LB only) at the highest concentration of antibiotic were passaged into fresh LB with antibiotic in a subsequent plate. A total of 5 serial passages were performed. For *P. aeruginosa*, LB + 0.01% tween 80 was used. For all species, antibiotics were diluted 2-fold down each given row in a 96 well plate. For sequencing of resistance loci from select evolution assays, gDNA was extracted from bacterial samples using GeneJet Genomic DNA Purification Kit (ThermoFisher). Samples were sequenced by Genewiz using custom primers.

Mutagenesis Measurements Post Epithelial Cell Infection

HELA cells were cultured in DMEM supplemented with 20% heat-inactivated FBS, 1% glutamine, and 1% penicillin/streptomycin at 37°C in 5% CO_2. The night before infection, $1x10^7$ HeLa cells were seeded into 15cm plates and incubated overnight. A single *S. typhimurium* colony from strain HM1996 (WT St19) or HM3429 (D*mfd*St19) was used to inoculate an overnight culture, grown in LB with appropriate antibiotic selection at 37°C 260rpm. The next morning, the overnight bacterial culture was set back to OD_{600} 0.05 and grown to mid-exponential phase. The bacteria were then washed twice with tissue culture grade 1X PBS and resuspended in an appropriate volume of DMEM + 20% FBS + 1% glutamine. Bacteria were then applied to the HeLa cells and allowed to invade for 60 minutes at 37°C 5% CO_2, at an MOI of 100:1. After 60 minutes of invasion, the bacteria were removed and fresh media applied to the HeLa cells. For ARM-1 treated conditions, the fresh media contained 31.25μM ARM-1. 30 minutes later, 50μg/mL gentamicin was added to the media to kill any remaining extracellular bacteria. After 8 hours of infection, HeLa cells were washed 2X with 1X PBS and lysed with 5mL 1% Triton-X-100 in water. A small portion of lysate was serially diluted and plated on LB for CFU enumeration. The remaining volume was plated on LB + 50mg/mL 5-fluorocytosine (5-FC) and grown overnight at 37°C to determine mutation frequency. Mutation frequency is reported as the ratio of number of colonies that grew on selection plates to the number of viable bacterial cells in each lysate.

Mammalian Cell Cytotoxicity

Cytotoxicity of ARM-1 against HeLa, Caco-2, and HEK293 cells was determined using CellTox Green Cytotoxicity Assay (Promega) according to manufacturer instructions. ARM-1 was diluted in DMSO and applied to the culture such that final concentrations of DMSO were less than 0.05%. Reported toxicity is relative to a DMSO only control. Cells were incubated with ARM-1 for 24 hours prior to addition of reporter dye. Fluorescence was read on a BioTek Synergy Neo plate reader.

Statistical Analysis

All statistical analysis was performed using GraphPad Prism 9.0.

Figure Design

All figures were created using GraphPad Prism 9.0, Adobe Illustrator, or BioRender.

Author Contributions and Affiliations

AEJ, HEB, AJHV, JCG, and ENS performed experiments. HM, AEJ, HEB, and JCG analyzed data. AEJ and JCG created figures. HM and AEJ wrote the manuscript. KK synthesized and validated ARM-1. HM conceived and directed the project.

Acknowledgments

Current and former Merrikh Lab members, especially Mark Ragheb and Maureen Thomason, the Vanderbilt Institute of Chemical Biology Molecular Design and Synthesis Center, the Vanderbilt Institute of Chemical Biology High Throughput Screening Core, VU Molecular Cell Biology Core, and Calibr at the Scripps Research Institute.

Funding Sources

This work was supported by the NIH R01-AI-127422, NIH R01-GM-127593, the Bill & Melinda Gates Foundation OPP1154551, and Vanderbilt University start-up funds to H.M, as well as Vanderbilt University support to the cores acknowledged. AEJ is supported by NIH 5T32CA009582-34.